Dynamic Functional Connectome Harmonics

Hoyt Patrick Taylor IV[1] and Pew-Thian Yap[2,3](✉)

[1] Department of Computer Science, University of North Carolina, Chapel Hill, NC, USA
[2] Department of Radiology, University of North Carolina, Chapel Hill, NC, USA
ptyap@med.unc.edu
[3] Biomedical Research Imaging Center, University of North Carolina, Chapel Hill, NC, USA

Abstract. Functional connectivity (FC) "gradients" enable investigation of connection topography in relation to cognitive hierarchy, and yield the primary axes along which FC is organized. In this work, we employ a variant of the "gradient" approach wherein we solve for the normal modes of FC, yielding functional connectome harmonics. Until now, research in this vein has only considered static FC, neglecting the possibility that the principal axes of FC may depend on the timescale at which they are computed. Recent work suggests that momentary activation patterns, or brain states, mediate the dominant components of functional connectivity, suggesting that the principal axes may be invariant to change in timescale. In light of this, we compute functional connectome harmonics using time windows of varying lengths and demonstrate that they are stable across timescales. Our connectome harmonics correspond to meaningful brain states. The activation strength of the brain states, as well as their inter-relationships, are found to be reproducible for individuals. Further, we utilize our time-varying functional connectome harmonics to formulate a simple and elegant method for computing cortical flexibility at vertex resolution and demonstrate qualitative similarity between flexibility maps from our method and a method standard in the literature.

Keywords: dynamic functional connectivity · harmonics · flexibility

1 Introduction

Nonlinear dimensionality reduction techniques such as diffusion embedding and principal component analysis applied to FC data provide the primary axes along which FC is organized [11]. Laplacian embedding is a related nonlinear dimensionality reduction technique, which yields the normal modes or functional connectome harmonics, which are the focus of this study. Connectome harmonics have a straightforward interpretation as the brain analog of the Fourier basis and can be used to filter the underlying fMRI signal.

A growing body of evidence suggests that the strongest components of FC are underpinned by brief but strong patterns of activation, or brain states, resembling the dominant components of FC (e.g., the default mode network) rather than sustained,

This work was supported in part by the United States National Institutes of Health (NIH) through grants MH125479 and EB008374.

H. Greenspan et al. (Eds.): MICCAI 2023, LNCS 14227, pp. 268–276, 2023.
https://doi.org/10.1007/978-3-031-43993-3_26

low-magnitude signal coherence between brain regions implicated in those strongest components of FC [3,10,14]. Simultaneously, few studies have analyzed how functional connectome harmonics depend on the timescale on which they are computed. If briefly activated brain states mediate the primary axes of FC, we would expect momentary functional connectome harmonics to be stable with respect to timescale.

The robustness of connectivity patterns across populations and the reliability and reproducibility of FC gradients across subjects and choices of parameters have been well studied [1,9,17]. However, it is not well understood to what degree the magnitude of and relationship between the activation timeseries of certain brain states is reproducible within and across subjects. Further, the reliability of time-varying FC harmonics has yet to be studied. Given both our hypothesis that functional connectome harmonics represent discrete brain states and evidence that discrete brain states underpin FC, we expect that the activation energy of principal functional connectome harmonics with respect to the underlying fMRI signal will be reproducible within individuals.

Previous work has shown that network configuration is dynamic during task and rest, with the community allegiance of brain regions changing over time [4]. The propensity of brain regions to change network allegiance, or flexibility, has been implicated in learning, development, and psychiatric disorders [2,8,19]. Previous studies have defined cortical flexibility in terms of the frequency of community allegiance change and demonstrated relationships between flexibility, learning, and development. Functional connectome harmonics correspond to axes along which connectivity is organized, yielding both a convenient basis to represent underlying functional activation and a spectral representation of each brain region. The spectral coordinates define the position of a brain region in terms of the primary axes of FC, with similar spectral coordinates indicating similar network allegiance profiles. By computing time-varying functional connectome harmonics, we can study the temporal dynamics of spectral coordinates, which provides a new lens through which to examine cognitive flexibility. Previous studies have relied on community detection algorithms to compute the degree of change in network allegiance of brain regions, which are hindered by free parameters governing the number of communities, the strength of connection between adjacent time points, and the choice of parcellation due to computational restraints on community detection algorithms. Dynamic functional connectome harmonics present a simpler method for computing flexibility: change in network allegiance—and therefore flexibility—is proportional to change in spectral coordinates given by connectome harmonics.

2 Methods

We used the resting-state fMRI time series of 44 subjects from the HCP minimal preprocessed test-retest dataset mapped to the 32k MSM-All surface atlas [7]. For each subject, the test and retest datasets contain data from two rs-fMRI sessions for a total of 176 sessions. To investigate the variation in of functional connectome harmonics at different time scales, we computed FC matrices at 4 window lengths: $w = 0.5$, 1, 2, and 3.5 min. For each window length, each 28 min time series was divided into $N_w = \frac{28}{w}$ windows, and an FC matrix was computed for each window. FC between two

surface vertices was computed as the correlation between the z-normalized time series. In light of studies demonstrating that thresholding FC matrices increases the reliability of FC gradients [9], the top 10% of the correlations for each row in each FC matrix was retained, and the FC matrices were made symmetric by taking the average of each matrix and its transpose.

For each FC matrix $\hat{A}(t)$ at timepoint t, the normalized graph Laplacian matrix, $\hat{L}(t) = \hat{D}(t)^{\frac{1}{2}}\hat{A}(t)\hat{D}(t)^{\frac{1}{2}}$, with $\hat{D}(t)_{i,i} = \sum_{j=0}^{N_v}\hat{A}(t)_{i,j}$ was computed. The first N_h eigenvectors of $\hat{L}(t)$, solutions to $\hat{L}(t)\boldsymbol{\psi}(t)_k = \lambda(t)_k\boldsymbol{\psi}(t)_k$, were computed, yielding the functional connectome harmonics of window t, $\hat{\psi}(t) = \{\boldsymbol{\psi}_k(t)|k = 1, \ldots, N_h\}$. Note that $\hat{\psi}(t)$ is a matrix of size $N_v \times N_h$, where each column is a harmonic $\boldsymbol{\psi}(t)_k$, N_v = 52,924 is the number of vertices, and N_h = 7 is the number of harmonics computed. This process is carried out for all windows for each acquisition, yielding the dynamic functional connectome harmonics for a particular subject and window length: $\{\hat{\psi}(t)|t = 1, \ldots, N_w\}$.

To extract a single set of harmonics for each acquisition at each window length, the window-wise harmonics from all windows for that acquisition were stacked horizontally into a large matrix of size $N_v \times (N_h N_w)$ on which PCA was performed, yielding one set of principal components for each acquisition and each subject. We refer to the components obtained via this approach as the most-prevalent harmonics, $\bar{\hat{\psi}}$, as they encapsulate orthogonal patterns of maximum variation across all window-wise harmonics. This process was also repeated on the group level for the test and retest cohorts separately at each window length, yielding the most prevalent harmonics $\bar{\hat{\Psi}}$ for the test and retest groups. For computation of $\bar{\hat{\Psi}}$, the matrix on which PCA was performed is of size $N_v \times (N_h N_w N_a N_s)$, where N_a = 2 is the number of acquisitions per subject for either test or retest, and N_s = 44 is the number of subjects.

To investigate the reproducibility of dynamic functional connectome harmonics as a basis for reconstructing the underlying fMRI signal, we utilize the harmonics as operators on functional timeseries. For a vertex-wise functional time series $\hat{X} = [\boldsymbol{x}(1), \ldots, \boldsymbol{x}(N_T)]$, where $\boldsymbol{x}(t)$ is the fMRI activation at timepoint t, we define its $N_h \times N_T$ spectral coefficient timeseries matrix $\hat{\alpha}$ with respect to harmonics $\hat{\psi}$ as

$$\hat{\alpha} = \hat{\psi}^{\top}\hat{X}, \tag{1}$$

where each row $\boldsymbol{\alpha}_k$ of $\hat{\alpha}$ is the spectral coefficient timeseries of timeseries $\hat{X}$ for harmonic $\boldsymbol{\psi}_k$. Each $\boldsymbol{\alpha}_k$ of $\hat{\alpha}$ gives the activation power of harmonic k at each time point, and the L2 norm of $\boldsymbol{\alpha}_k$ yields the activation energy $E(\boldsymbol{\psi}_k, \hat{X}) = ||\boldsymbol{\alpha}_k||$ of harmonic k across the entire timeseries. Further, we define the harmonic-filtered timeseries $\tilde{\hat{X}}$ and the representation efficiency ratio γ as

$$\tilde{\hat{X}} = (\hat{\alpha}^{\top}\hat{\psi}^{\top})^{\top}; \quad \gamma = \frac{||\tilde{\hat{X}}||}{||\hat{X}||}. \tag{2}$$

A set of harmonics $\{\boldsymbol{\psi}_k|k = 1, \ldots, N_h\}$ defines a spectral coordinate vector $\boldsymbol{\xi}^i = [\psi^i_1, \ldots, \psi^i_{N_h}]$ for each vertex i on the surface, specifying a position in the harmonic embedding space. To allow for comparison of spectral coordinates across a series

of consecutive time windows, we first compute the most-prevalent harmonics $\bar{\hat{\psi}}$ of the time series, and perform Procrustes alignment [18] between each set of window-wise harmonics $\hat{\psi}(t)$ and the most-prevalent harmonics $\bar{\hat{\psi}}$ from that acquisition using the implementation from [17]. These aligned harmonic time series define a trajectory in spectral space for each vertex. Vertices that have similar network allegiance have similar spectral coordinates, taking on similar values in each harmonic. A large change in spectral coordinates between timepoints t and $t+1$ indicates a change in FC topology relative to that vertex. We therefore define flexibility in terms of the distance between spectral coordinates at consecutive time points. For N_w sets of aligned harmonics computed at consecutive windows, we define the flexibility of vertex i as

$$f^i = \left(\sum_{t=1}^{N_w - 1} ||\boldsymbol{\xi}^i(t) - \boldsymbol{\xi}^i(t+1)||^2 \right)^{\frac{1}{2}}. \tag{3}$$

In order to evaluate our method of computing flexibility, we also employ a standard community detection based technique for comparison with our method wherein a graph modularity metric is optimized to obtain a community partition using a multi-layer temporal graph [2,13]. Due to computational complexity of the modularity optimization process involved, we apply this standard flexibility metric to FC data parcellated using the FreeSurfer Destrieux Atlas [5].

3 Results

Our most-prevalent harmonics comprise meaningful patterns of activation on the cortex (Fig. 1). On the group level, $\bar{\boldsymbol{\Psi}}_1$ reflects the default mode network (DMN) and $\bar{\boldsymbol{\Psi}}_2$ the task positive network (TPN) [6]. Our harmonics largely resemble FC gradients computed in the literature, although we do not observe the visual vs somatosensory component, which has been observed as the second gradient in static FC studies [11,17]. The absence of this harmonic at shorter timescales may indicate that it is mediated by longer-term, lower magnitude signal co-fluctuations and within visual and somatosensory cortices.

We evaluated the stability of the group level most-prevalent harmonics across repeated measurements (test and retest group cohorts) and across varying window length using cosine similarity and found high similarity ($\geq$0.70) between all pairings, indicating high stability (Fig. 1). Further, we evaluated the intra-subject stability of the individual most-prevalent harmonics using cosine similarity and found high stability across repeated measurements (4 scans per subject) for the first 3 harmonics. Table 1 displays the mean $\pm$ the standard deviation of the intra-subject cosine similarity between individual most-prevalent harmonics, and of the inter-window cosine similarity between dynamic harmonics of a given subject for $k = 1, 2, 3$. Note that individual most-prevalent and dynamic harmonics were Procrustes aligned before comparison in Table 1.

We investigated how the harmonics relate to functional timeseries by examining the stability of the harmonic activation energy of the first two harmonics, $||\boldsymbol{\alpha}_1||$ and $||\boldsymbol{\alpha}_2||$, the representation efficiency ratio γ, and the correlation between $\boldsymbol{\alpha}_1$ and $\boldsymbol{\alpha}_2$. For

Table 1. Intra-subject and inter-window cosine similarity in harmonics

	intra-subject $\bar{\psi}_k$			inter-window $\psi(t)_k$		
w	$k=1$	$k=2$	$k=3$	$k=1$	$k=2$	$k=3$
0.5	0.81 ± 0.11	0.79 ± 0.10	0.72 ± 0.13	0.22 ± 0.10	0.17 ± 0.08	0.12 ± 0.06
1	0.83 ± 0.09	0.80 ± 0.09	0.74 ± 0.11	0.41 ± 0.12	0.33 ± 0.11	0.25 ± 0.09
2	0.84 ± 0.09	0.82 ± 0.09	0.75 ± 0.11	0.58 ± 0.11	0.50 ± 0.12	0.40 ± 0.12
3.5	0.86 ± 0.07	0.82 ± 0.09	0.76 ± 0.11	0.70 ± 0.09	0.61 ± 0.11	0.52 ± 0.12

Table 2. Reliability of harmonic decomposition metrics

	$\|\|\boldsymbol{\alpha}_1\|\|$	$\|\|\boldsymbol{\alpha}_2\|\|$	$\rho(\boldsymbol{\alpha}_1, \boldsymbol{\alpha}_2)$	γ
ICC	$0.68 \pm .12$	$0.59 \pm .13$	$0.64 \pm .12$	$0.58 \pm .13$
p	1.1×10^{-16}	5.85×10^{-14}	2.22×10^{-16}	1.3×10^{-15}
F-stat	7.85	5.59	6.60	6.20

each session and each subject, we computed each quantity using the most-prevalent harmonics $\bar{\bar{\psi}}$ of that subject and session and investigated the reliability of these harmonic-derived metrics using the intraclass correlation coefficient (ICC), with results summarized in Table 2. ICC results indicate larger variability in each metric across subjects than across sessions with high significance ($p \leq 1 \times 10^{-13}$ for all metrics), with moderate to good reliability for $||\boldsymbol{\alpha}_1||$ and $\rho(\boldsymbol{\alpha}_1, \boldsymbol{\alpha}_2)$, and moderate reliability for $||\boldsymbol{\alpha}_2||$ and γ. We also found that $\rho(\boldsymbol{\alpha}_1, \boldsymbol{\alpha}_2)$ had a mean of –0.153 and standard deviation of .07, indicating that the activation timecourses of the harmonics most closely resembling the DMN and TPN are anticorrelated.

We computed flexibility using our dynamic functional connectome harmonic formulation (Eq. 3) for each subject and session for each window length. Average flexibility computed using $w = 2$ is displayed in Fig. 2a. Importantly, there were not significant differences in the qualitative map of flexibility with varying window length. As a sanity-check on our definition of flexibility, we also computed flexibility using traditional methods from the literature [2,8,14,19], using the Leidenalg community detection algorithm [15] with interlayer connection strength $\omega = 1$ and resolution parameter $r = 1$, and window length $w = 2$. Flexibility was computed as the ratio of the total number of community assignment changes to the total number of possible transitions for each node (parcel). Using the community-detection based flexibility approach, we find very similar distribution of flexibility values, but with higher values in the prefrontal cortex, and slightly lower values in the occipital cortex. Flexibility results from both methods with the exception of the high values in the occipital cortex are in keeping with previous studies on flexibility, indicating that our definition of flexibility is an effective method for measuring the propensity of brain regions to change community allegiance [12]. Importantly, our definition of flexibility involves fewer parameters than conventional methods, and yields a vertex-wise map of flexibility.

4 Discussion

Individual most-prevalent harmonics are found to be similar across acquisitions after Procrustes alignment, while there is notably lower average similarity between dynamic harmonics, particularly at shorter timescales (Table 1). This is not unexpected, as we anticipate variability in FC between windows. Higher intra-subject similarity in $\bar{\psi}_k$ compared with inter-window $\psi(t)_k$ similarity indicates that our PCA-based method of extracting the most-prevalent harmonics from the dynamic harmonics achieves its goal of extracting the common brain states for a given acquisition and that those states are reproducible within subjects. Further, our most-prevalent harmonics are advantageous over naive averaging approaches, as they preserve the orthogonality constraint intrinsic to connectome harmonics.

Our most-prevalent functional connectome harmonics show invariance under change in timescale and strongly resemble FC "gradients" in the literature computed on static FC [11]. As connectome harmonics represent the primary axes along which FC is organized, their invariance to timescale is significant: persistence of the same harmonics at long, medium, and short timescales supports the hypothesis that the harmonics themselves are brain states whose activation fluctuates. Notably, at the group level, our second harmonic $\bar{\boldsymbol{\Psi}}_2$ resembles the TPN, whereas in the literature the second gradient is found to be an axis spanning from visual to somatosensory areas. Although our $\bar{\boldsymbol{\Psi}}_3$ has high intensity values in the visual cortex, it is not a clear axis between visual and somatosensory regions. This difference between our results and static FC gradient results may indicate that the second FC gradient from the literature is the result of longer-timescale, lower-magnitude signal variations that differentiate the visual and somatosensory cortices.

Our analysis indicates that our individual most-prevalent harmonics $\bar{\hat{\psi}}$ are a reproducible basis with which to decompose the underlying fMRI signal. The projection coefficient timeseries of a given harmonic, $\boldsymbol{\alpha}_k$, represents the timecourse of relative activation of $\bar{\psi}_k$. Importantly, we found that the magnitude of these activation timecourses for the first and second most-prevalent harmonic (corresponding to the DMN and TPN), as well as the correlation between them were reliable across repeated measurements in individual subjects, with significantly higher variability across subjects than across scans (Table 2).This indicates that the strength of activation and the temporal relationship between the activation of $\bar{\psi}_1$ and $\bar{\psi}_2$ are reliable, and suggests that our method of extracting most-prevalent harmonics provides a reliable subject-specific method for analyzing the manifestation and relationship between different connectivity patterns. It is also worth noting that we found that $\rho(\boldsymbol{\alpha}_1, \boldsymbol{\alpha}_2)$ was negative in general, indicating that activation of the DMN and TPN is anticorrelated, in keeping with previous studies [6,16]. In light of this, further analysis of the strength of activation of meaningful harmonics and their interrelationships could provide meaningful insights into differences in network dynamics in diseased populations.

Our dynamic functional connectome harmonic definition of flexibility yields a vertex-wise map of cortical flexibility for each subject, requires fewer parameters, and is less computationally expensive than standard definitions of flexibility. Our group-average flexibility result (Fig. 2a) shows strong resemblance to the result computed using the community-detection based flexibility definition (Fig. 2b). Transmodal

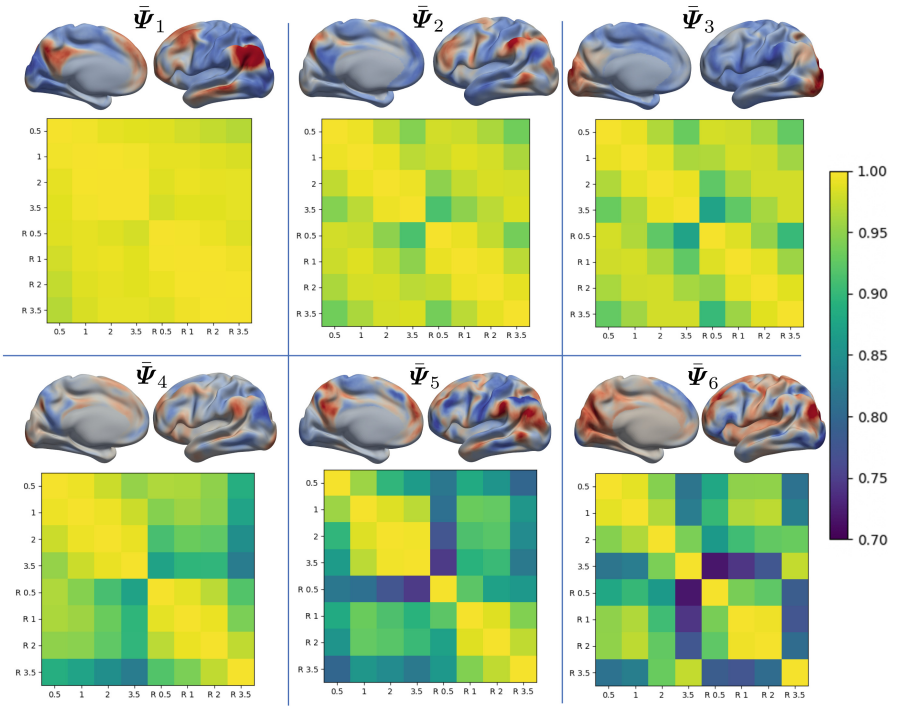

Fig. 1. Group-level most-prevalent harmonics $\bar{\Psi}_k$ derived from 2 min window for test cohort mapped to the cortical surface. Matrix below each $\bar{\Psi}_k$ is cosine similarity between group-level harmonics computed for different window lengths and test or retest cohort. Matrix labels are window length in minutes, with R denoting retest cohort. $\bar{\Psi}_1$ differentiates the default mode network from the rest of the brain, $\bar{\Psi}_2$ differentiates regions in the task positive network from the rest of the brain. Color bar ranges from cosine similarity of 0.70 to 1.00.

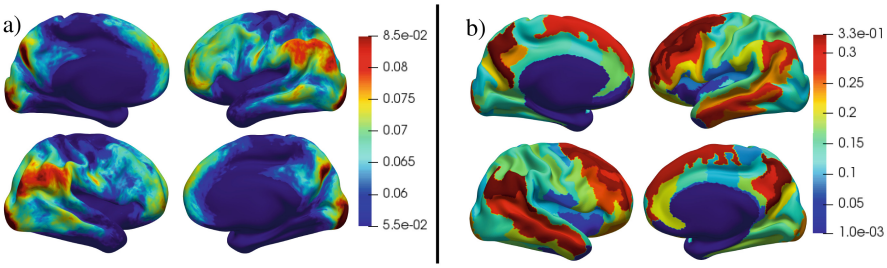

Fig. 2. Group average flexibility computed using **a)** dynamic functional connectome harmonic method (Eq. 3) and **b)** conventional community detection based method. Note that both flexibility maps are computed using 2 min window length.

regions such as the angular gyrus, temporal-parietal junction, prefrontal and medial prefrontal cortices, precuneus, and middle temporal gyrus display high flexibility due to their involvement in complex high order cognitive functions. In contrast, unimodal regions such as motor, somatosensory, limbic, and auditory cortex demonstrate low flexibility. An interesting feature of our flexibility result is high flexibility in the visual cortex. Although this has not been consistently found in previous studies, it is worth noting that many of the seminal works on flexibility deal with task-based fMRI data [2, 14], wherein flexibility in the visual cortex may be lower than at rest. One possible explanation is that during rest, daydreaming and imagination lead to rapid switching in the recruitment of the visual cortex, leading to high flexibility values.

5 Conclusion

Our most-prevalent functional connectome harmonics and their dynamic counterparts provide a powerful lens through which to study the organization of FC as well as its dynamics. We demonstrate that the most-prevalent harmonics are invariant when the timescale at which their underlying connectivity matrices are computed is changed, and that they are highly stable across repeated measurements on the group and individual level. Further, we show that our harmonics provide a reliable basis with which to filter fMRI timeseries and to extract the activation timecourses of individual harmonic brain states. Importantly, the reproducibility of these harmonic decompositions indicates that they provide a subject-specific method with which to study the dynamics of specific brain states and their interrelationships. We also present a novel formulation of cortical flexibility defined in terms of dynamic functional connectome harmonics and show that it gives vertex resolution flexibility maps that qualitatively similar results to previous definitions of flexibility which are constrained by free parameters and computational complexity.

References

1. Abrol, A., et al.: Replicability of time-varying connectivity patterns in large resting state fMRI samples. Neuroimage **163**, 160–176 (2017). https://doi.org/10.1016/j.neuroimage.2017.09.020
2. Bassett, D.S., Wymbs, N.F., Porter, M.A., Mucha, P.J., Carlson, J.M., Grafton, S.T.: Dynamic reconfiguration of human brain networks during learning. Proc. Natl. Acad. Sci. U.S.A. **108**, 7641–7646 (2011). https://doi.org/10.1073/pnas.1018985108
3. Betzel, R.F., Faskowitz, J., Sporns, O.: High-amplitude co-fluctuations in cortical activity drive resting-state functional connectivity (2019). https://doi.org/10.1101/800045
4. Cohen, J.R.: The behavioral and cognitive relevance of time-varying, dynamic changes in functional connectivity (2018). https://doi.org/10.1016/j.neuroimage.2017.09.036
5. Destrieux, C., Fischl, B., Dale, A., Halgren, E.: Automatic parcellation of human cortical gyri and sulci using standard anatomical nomenclature. Neuroimage **53**, 1–15 (2010). https://doi.org/10.1016/j.neuroimage.2010.06.010
6. Fox, M.D., Snyder, A.Z., Vincent, J.L., Corbetta, M., Van Essen, D.C., Raichle, M.E.: The human brain is intrinsically organized into dynamic, anticorrelated functional networks. Proc. Natl. Acad. Sci. U.S.A. **102**, 9673–9678 (2005). https://doi.org/10.1073/pnas.0504136102

7. Glasser, M.F., et al.: The minimal preprocessing pipelines for the human connectome project. Neuroimage **80**, 105–124 (2013). https://doi.org/10.1016/j.neuroimage.2013.04.127
8. Harlalka, V., Bapi, R.S., Vinod, P.K., Roy, D.: Atypical flexibility in dynamic functional connectivity quantifies the severity in autism spectrum disorder. Front. Hum. Neurosci. **13**, 6 (2019). https://doi.org/10.3389/fnhum.2019.00006
9. Hong, S.J., et al.: Toward a connectivity gradient-based framework for reproducible biomarker discovery. Neuroimage **223**, 117322 (2020). https://doi.org/10.1016/j.neuroimage.2020.117322
10. Liu, X., Zhang, N., Chang, C., Duyn, J.H.: Co-activation patterns in resting-state fMRI signals (2018). https://doi.org/10.1016/j.neuroimage.2018.01.041
11. Margulies, D.S., et al.: Situating the default-mode network along a principal gradient of macroscale cortical organization. Proc. Natl. Acad. Sci. U.S.A. **113**, 12574–12579 (2016). https://doi.org/10.1073/pnas.1608282113
12. Mattar, M.G., Betzel, R.F., Bassett, D.S.: The flexible brain (2016). https://doi.org/10.1093/brain/aww151
13. Mucha, P.J., Richardson, T., Macon, K., Porter, M.A., Onnela, J.P.: Community structure in time-dependent, multiscale, and multiplex networks. Science **328**, 876–878 (2010). https://doi.org/10.1126/science.1184819
14. Reddy, P.G., et al.: Brain state flexibility accompanies motor-skill acquisition. Neuroimage **171**, 135–147 (2018). https://doi.org/10.1016/j.neuroimage.2017.12.093
15. Traag, V.A., Waltman, L., van Eck, N.J.: From Louvain to Leiden: guaranteeing well-connected communities. Sci. Rep. **9**, 5233 (2019). https://doi.org/10.1038/s41598-019-41695-z
16. Uddin, L.Q., Kelly, A.M., Biswal, B.B., Castellanos, F.X., Milham, M.P.: Functional connectivity of default mode network components: correlation, anticorrelation, and causality. Hum. Brain Mapp. **30**, 625–637 (2009). https://doi.org/10.1002/hbm.20531
17. Vos de Wael, R., et al.: BrainSpace: a toolbox for the analysis of macroscale gradients in neuroimaging and connectomics datasets. Commun. Biol. **3**, 103 (2020). https://doi.org/10.1038/s42003-020-0794-7
18. Wang, C., Mahadevan, S.: Manifold alignment using procrustes analysis. In: Proceedings of the 25th International Conference on Machine Learning (2008). https://doi.org/10.1145/1390156.1390297
19. Yin, W., et al.: The emergence of a functionally flexible brain during early infancy. Proc. Natl. Acad. Sci. U.S.A. **117**, 23904–23913 (2020). https://doi.org/10.1073/pnas.2002645117